A Lattice Design for the CLIC Damping Ring

Maxim Korostelev and Frank Zimmermann
CERN, Geneva, Switzerland

1 INTRODUCTION

A high-energy (0.5-5.0 TeV centre of mass) electron-positron Compact Linear Collider (CLIC) is being studied at CERN as a new physics facility [1]. The design study has been optimized for 3 TeV centre-of-mass energy. Intense bunches injected into the main linac must have unprecedentedly small emittances to achieve the design luminosity $10^{35} cm^{-2} s^{-1}$ required for the physics experiments. The positron and electron bunch trains will be provided by the CLIC injection complex.

To decouple the wide aperture requirements for the incoming positron beam from the final emittance requirements of the main linac, a pre-damping ring with a large dynamic acceptance and relatively large equilibrium emittance is used to pre-damp the incoming beam, as is shown in Fig. 1.

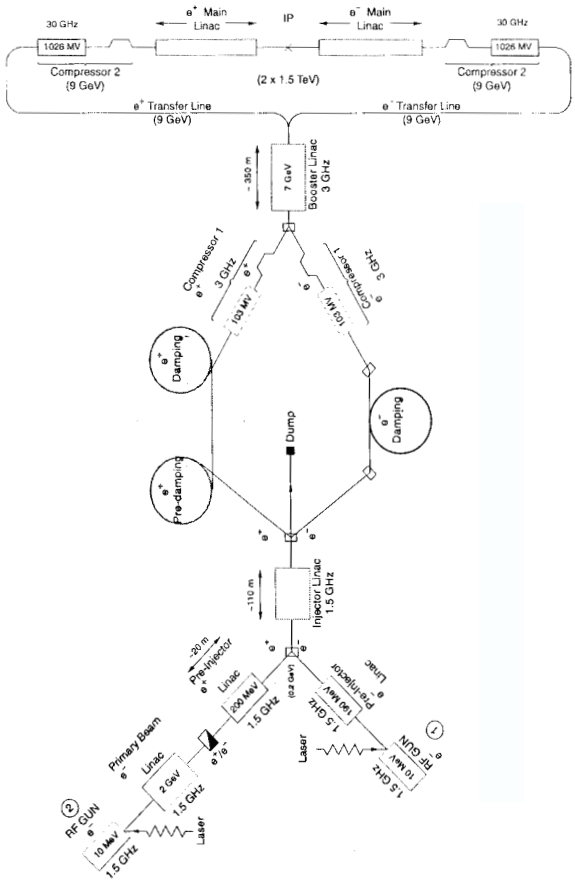

Figure 1: The CLIC layout [1].

In the case of electron production, taking into account the incoming normalized emittance of 7000 nm rad provided by the high brilliance injector linac, a single ring similar to the final positron damping ring will be sufficient.

In the report, the main positron DR optics producing such low-emittance beam is described.

2 EVOLUTION OF E^+ OR E^- BEAM EMITTANCES

The evolution of electron(positron) beam emittances in the damping ring is defined by the interplay of radiation damping, quantum excitation, and intra-beam scattering (IBS). A change in the momentum deviation of a particle in a dispersive region results in a change of its betatron oscillation amplitude.

Ignoring the effect of the opening angle [2], which is still weak for CLIC parameters and beta functions below 10 m, an increase of the transverse beam emittance through quantum excitation occurs only when synchrotron radiation is emitted at a place with nonzero dispersion. The emittance growth due to IBS is similar, but in contrast to synchrotron radiation it also arises outside of the bending magnets.

The horizontal ε_x, vertical ε_y and longitudinal ε_t emittances evolve with time according to a set of three coupled differential equations:

$$\dot{\varepsilon}_\mu = -\frac{2}{\tau_\mu}(\varepsilon_\mu - \varepsilon_{\mu 0}) + \frac{2\varepsilon_\mu}{T_\mu(\varepsilon_x, \varepsilon_y, \varepsilon_t)},\ \mu \in \{x, y, t\} \quad (1)$$

The three differential equations (1) are coupled through the IBS growth times $T_\mu(\varepsilon_x, \varepsilon_y, \varepsilon_t),\ \mu \in \{x, y, t\}$, which are non-linear functions of emittances. The equilibrium emittances follow from solution of this equation There are two well known formalisms for computing the IBS growth times $T_\mu(\varepsilon_x, \varepsilon_y, \varepsilon_t)$, namely the Bjorken-Mtingwa theory [3] and Piwinski's theory [4]. Both approaches determine the local, two-particle Coulomb scattering.

In practice the vertical emittance is limited by nonzero betatron coupling, by residual vertical dispersion, and by IBS.

3 CLIC DAMPING RING OPTICS

Since CLIC will likely operate with polarized beams, the damping ring must maintain a high spin polarization. Therefore, the ring energy should be chosen so that the spin tune is a half integer to stay away from the strong integer spin resonance. The energy for the damping ring was chosen as 2.42 GeV that corresponds to the spin tune of 5.5. At the next possible lower energy of 1.98 GeV, the IBS is too strong, since the IBS growth time is proportional to $\sim \gamma^4$, while damping time is inversely proportional to $\sim \gamma^3$.

The horizontal normalized emittance without IBS can be presented by the expression (2) given for the Theoretical Minimum Emittance (TME) lattice [5, 6, 7, 8, 9, 12, 13]. Such lattice is most suitable for the low emittance compact arc cell. The length of a cell is important since the damping time is directly proportional to the ring circumference.

A TME cell is composed of one bending magnet of length L and angle θ and, usually, three or four quadrupole magnets. The minimum horizontal emittance of TME cell with a small bending angle ($\theta \ll 1$) is given by [5]

$$\gamma\varepsilon_{x0m} \approx \frac{C_q\ \gamma^3\ \theta^3}{12\ \sqrt{15}} \left[\frac{1 - \frac{\theta^2(1+K_1\rho^2)}{23.33} + o[(K_1\theta)^4]}{1 - \frac{\theta^2(1+K_1\rho^2)}{6} + o[(K_1\theta)^4]} \right] \quad (2)$$

where K_1 is the normalized gradient in the bending magnet, and $C_q = 3.84 \times 10^{-13}$ m. The emittance is minimum when horizontal beta β_x and dispersion η_x functions at the center of the bend have the following optimum values at zero derivate ($\beta_x' = 0, \eta_x' = 0$) there:

$$\beta_m = \frac{L}{2\ \sqrt{15}}, \qquad \eta_m = \frac{L\ \theta}{24} \quad (3)$$

If beta and dispersion functions at the dipole center do not correspond to optimum value β_m and η_m then emittance is increased to the detuning factor ε_r times $\varepsilon_{x0} = \varepsilon_r\varepsilon_{x0m}$ where ε_r is given by [7]

$$\varepsilon_r = \frac{\sqrt{15}}{2}\ \frac{\eta}{\beta\theta} \left[\frac{\eta\ 24}{L\theta} - 2 \right] + \frac{9}{4} \left[\frac{L}{4\beta\ \sqrt{15}} + \frac{4\beta\ \sqrt{15}}{9\ L} \right]$$

This equation is plotted in Fig. 2 (bottom). The dispersion is maximum for a fixed value of the emittance deturning factor ε_r, when the horizontal beta function is equal to

$$\beta = \frac{L}{2\ \sqrt{15}}\ \varepsilon_r\ ,$$

where the dispersion becomes

$$\eta_{\max} = \frac{L\ \theta}{24} \left(1 + \frac{2}{\sqrt{5}} \sqrt{\varepsilon_r^2 - 1} \right)\ .$$

We now assume the values of β and η at the center of the bend given in equations stated here. Then the dependence of the horizontal phase advance per TME cell on the emittance detuning factor can be expressed by [9]

$$\mu_x = 2 \arctan \frac{\varepsilon_r\sqrt{3}}{\sqrt{\varepsilon_r^2 - 1} - \sqrt{5}}$$

This is plotted in Fig. 2 (top). If we compare the minimum emittance of the TME lattice with the minimum emittances produced by three other lattice types (Double Focusing Achromat, Triplet Achromat Lattice, Triple Bend Achromat) [10] for a fixed bending angle θ, we obtain the following ratios:

$$\frac{\varepsilon_{DFA}^{min}}{\varepsilon_{TME}^{min}} = 3, \qquad \frac{\varepsilon_{TAL}^{min}}{\varepsilon_{TME}^{min}} = 12, \qquad \frac{\varepsilon_{TBA}^{min}}{\varepsilon_{TME}^{min}} = \frac{7}{3}\ .$$

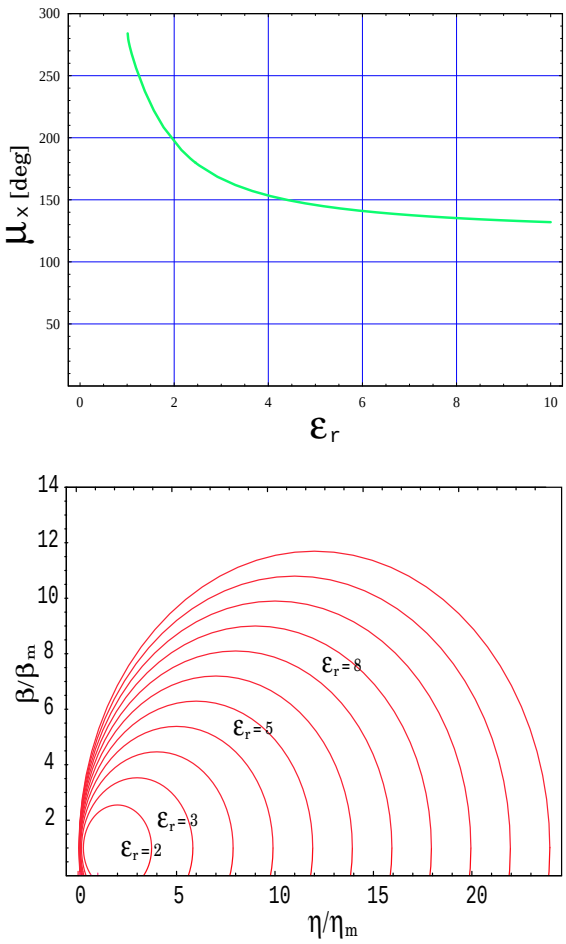

Figure 2: Horizontal phase advance per TME cell versus emittance detuning factor (top), and dispersion versus beta function at the center of bend of TME cell for 11 emittance detuning factors $\varepsilon_r \in \{2, 3, 4, 5...11\}$ (bottom)

A TME arc cell of the CLIC damping ring comprises four quadrupoles and a combined function bending magnet. The optics of this arc cell is shown in Fig. 3. The emittance detuning factor for this cell is $\varepsilon_r = 1.7$. The defocusing gradient in the bending magnet decreases the emittance via the associated change of horizontal damping partition. The combined function magnet also decreases the length of arc cell, that is 1.73 m. The defocusing gradient of the bending magnet is 24.73 kG/m. Phase advance per the cell is 210 degree and 90 degree for the vertical and horizontal motion respectively. In consideration of IBS, such phase advances give acceptable final emittances and, moreover, they allow the assembly of a second-order achromat for sextupolar chromatic correction.

The damping ring has two arcs connected by dispersion-free straight sections that include RF cavities, FODO cells with wigglers, and injection/extraction sections. The wiggler modules are located between quadrupole magnets in a FODO structure.

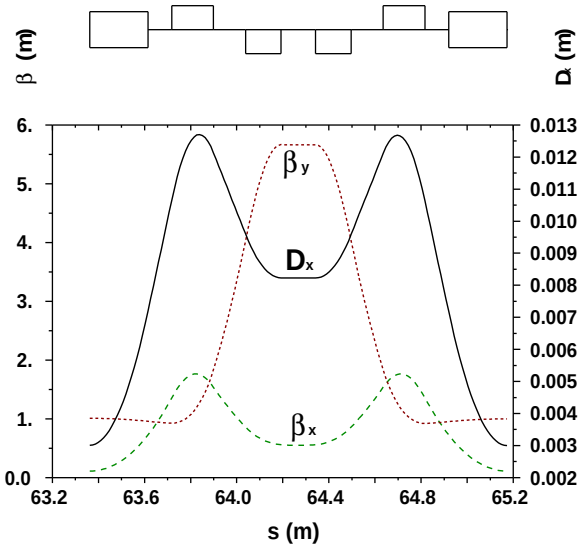

Figure 3: Dispersion and beta functions over the damping ring TME arc cell and the table of cell parameters

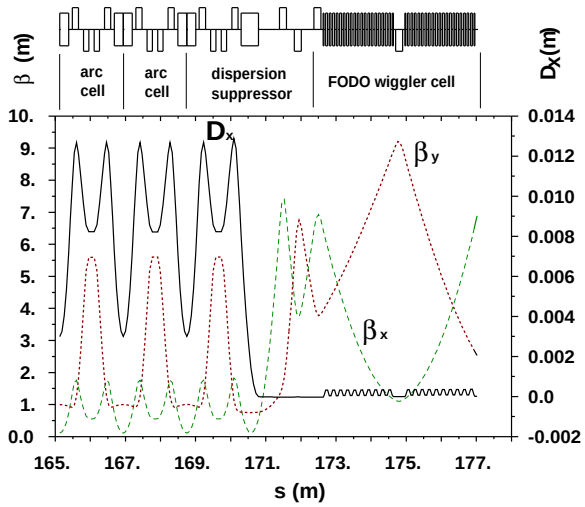

Figure 4: Dispersion and beta functions from arc cells to FODO cells with wigglers and the table of wiggler parameters

Table 1: Arc cell parameters

Parameter	Symbol	Value
Nominal e^+ ring energy	γmc^2	2.424
Number of cells	N_{cells}	96
Field of bending magnet	B_a	9.32 [kG]
Gradient field of bending magnet	G_a	-24.73 [kG/m]
Length of bending magnet	L	0.545 [m]
Phase advance per arc cell	μ_x/μ_y	210°/90°
Bending curvature	ρ	8.67 [m]
Length of arc cell	L	1.73 [m]

Table 2: Wiggler parameters

Parameter	Symbol	Value
Magnetic field of wiggler	B_w	17.64 [kG]
Wiggler period	λ_w	20 [cm]
Length of wiggler	L	2.1 [m]
Number of magnetic poles	N_p	21 pairs
Number of wigglers	N_w	76
Total length of wigglers	L_w	160 [m]

The phase advance of a FODO cell is $125°/92°$ for the horizontal and vertical motion, respectively. The wiggler sections do not perturb the emittance produced by the arcs. At the same time the wigglers considerably decrease the damping times. Consequently the damping times become less than the IBS growth times. The wiggler sections include a total of 76 wigglers, each of them 2.1 m long and consisting of 21 pairs of magnetic poles. The wiggler period is 20 cm.

The transverse damping times and the horizontal emittance in the presence of a wiggler disregarding IBS can be represented by the following expression (for $J_x = 1$) [11]

$$\frac{\varepsilon_{xw}}{\varepsilon_{x0}} = \frac{1 + \frac{5}{6\pi}\, G_a\, \frac{\langle\beta_x\rangle}{\rho}\, \frac{E^2}{\varepsilon_{x0}}\, (\frac{\rho}{\rho_w})^2 N_w\, N_p \Theta_w^3}{1 + \frac{2}{\pi}\, \frac{\rho}{\rho_w}\, N_w\, N_p \Theta_w}$$

$$\frac{\tau}{\tau_w} = \frac{1 + \frac{\rho L_w}{2\pi} \left(\frac{B_w}{3.356[\frac{Tm}{GeV}]E}\right)^2}{1 + \frac{L_w}{L_a}}$$

where $G_a = 1.46 \cdot 10^{-6}[mGeV^{-2}]$, L_a and $\langle\beta_x\rangle$ are the total length of the arcs and the average beta function over the wiggler respectively. Without IBS consideration and for the damping-ring parameters presented in Tables 1–2, the dependences of the relative damping time and relative horizontal emittance on the wiggler field and the pole length are presented in Figure 5. The subindex $x0$ refers to the case without wiggler sections (only arcs). The two top pictures in Fig. 5 refer to two different values of the average horizontal beta function $\langle\beta_x\rangle$ over the length of the wiggler. In the limit of many wiggler poles, the wigglers will not increase the horizontal emittance produced by arcs, if the average horizontal beta function is less than [11]

$$\langle\beta_x\rangle \leq \frac{384}{275}\sqrt{3}\, \frac{(mc^2)^3}{\hbar c e^3}\, \frac{16\varepsilon_{x0}E}{\lambda_w^2 B_w^3}\ .$$

4 DAMPING RING PARAMETERS AND FINAL BEAM EMITTANCES

Taking into account IBS, the values of the equilibrium transverse beam emittances ε_x, ε_y, rms energy spread σ_δ and rms bunch length σ_s were calculated for the proposed damping ring design by a step-wise integration in time. Computing the IBS growth rates by the Bjorken-Mtingwa formalism, we obtain the results summarized in Table 3. The design parameters of the damping ring are also presented in Table 3 (top).

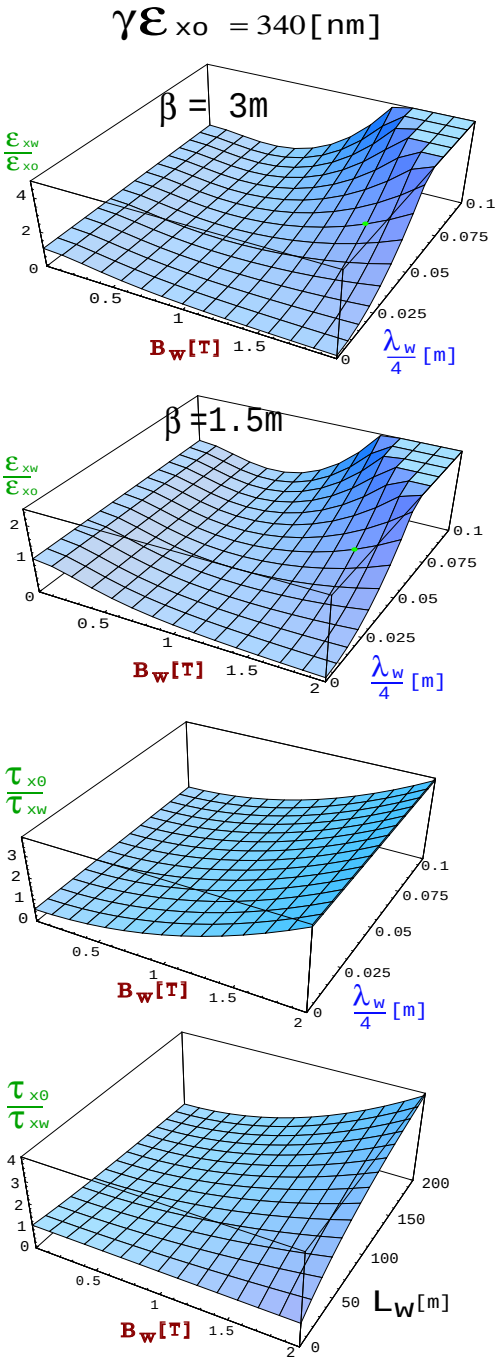

Figure 5: The dependences of the relative damping time τ_{x0}/τ_{xw} and relative horizontal emittance $\varepsilon_{xw}/\varepsilon_{x0}$ on the wiggler field B_w, total wiggler length L_w, and pole length $\lambda_w/4$. The top pictures also illustrate the effect of varying the beta function; the bottom pictures are for $< \beta_x >= 3m$.

The time evolution of ε_x, ε_y, σ_δ and σ_s between the injection (inj) and the final equilibrium beam at the moment of extraction, computed from the differential equations (1), are shown in Fig. 6. We observe that IBS increases the equilibrium horizontal emittance ε_{x0} about two times. On the positive side, the final horizontal emittance $\gamma\varepsilon_x$ of 620 [nm] produced by the damping ring at extraction woudl still be acceptable for the CLIC interaction point; at the interaction point $\gamma\varepsilon_x$ should not exceed 700 nm. However, additional emittance dilutions are expected in the linac and bunch compressors. The vertical normalized emittance of almost 9 nm is three times larger than the ideal target value of 3 nm. As for the horizontal plane, it remains smaller than the design emittance at the collision point (10 nm). The rms bunch-length σ_s and energy spread σ_δ at extraction correspond to a longitudinal emittance of 4280 eV m, which is compatible the maximum value required for the subsequent bunch compressors (4870 eV m). Figure 6 demonstrates that the equilibrium emittances are obtained after 20 ms. The beam in the ring consists of 9 trains and the repetition rate of the 3-TeV collider is 100 Hz. Thus each bunch is stored for 45 ms, and no transient effects from the damping are expected.

Table 3: List of CLIC damping ring parameters

Parameter	**Symbol**	**Value**
Nominal ring energy	γmc^2	2.424
No. of bunche trains stored	N_{train}	9
Ring circumference	C	357.2 [m]
Number of cells	N_{cells}	96
Extracted hor. emittance at IBS	$\gamma\varepsilon_x$	620 [nm]
Extracted vert. emittance at IBS	$\gamma\varepsilon_y$	8.7 [nm]
Extracted long. emittance at IBS	$\gamma mc^2\varepsilon_t$	4319 [eV×m]
Extracted energy spread at IBS	σ_δ	1.36×10^{-3}
Extracted bunch length at IBS	σ_s	1.31 [mm]
H. IBS equilibrium growth time	T_{xibs}	3.2 [msec]
L. IBS equilibrium growth time	T_{tibs}	5.1 [msec]
V. IBS equilibrium growth time	T_{yibs}	33.7 [msec]
Damping time	τ_x	2.62 [msec]
Damping time	τ_y	2.63 [msec]
Damping time	τ_t	1.32 [msec]
H. betatron tune	Q_x	72.85
V. betatron tune	Q_y	34.82
Betatron coupling	$\varepsilon_{y0}/\varepsilon_{x0}$	2.1%
Field of bending magnet	B_a	9.32 [kG]
Length of bending magnet	L	0.545 [m]
Phase advance per arc cell	μ_x/μ_y	210°/90°
Field of wiggler	B_w	17.64 [kG]
Momentum compaction	α_p	0.731×10^{-4}
Energy loss per turn	U_0	2.1916 [MeV]
RF frequency	f_{rf}	1500 [HHz]
RF voltage	V_m	3.0 [MV]
Revolution time	T_r	1.191 [μs]
Harmonic number	h	1786

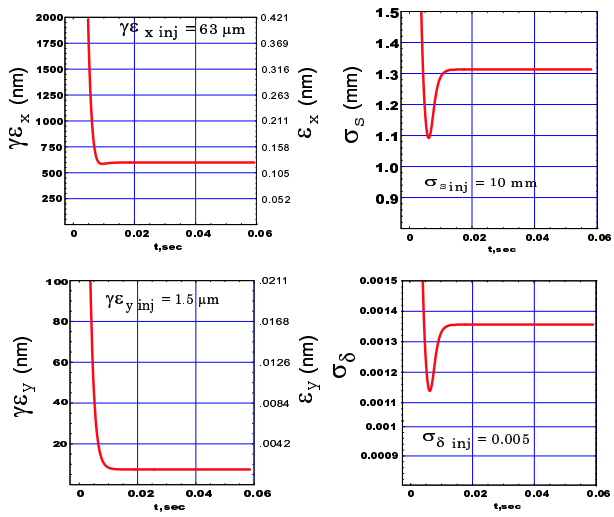

Figure 6: The evolution of beam emittances from injection values to equilibrium values

5 CHROMATICITY CORRECTION AND DYNAMIC APERTURE

Sextupoles introduce both second order geometric aberrations and chromatic aberrations. If two sextupoles of equal strength are placed at the entrance and exit of a $-I$ transformer the geometric aberrations introduced by the two sextupoles exactly cancel each other. A perfect cancellation of the second-order geometric aberrations produced by the sextupoles would be to place separate $-I$ transformers of sextupole pairs in such a way that they do not interfer with each other.

In our case this ideal scheme is impossible to realize, because there is not enough space available to arrange non-interlaced $-I$ transformers. The small beta and dispersion functions require a sufficient number of sextupoles in order to correct the large horizonal and vertical chromaticities. Therefore, in the proposed damping ring design, interlaced

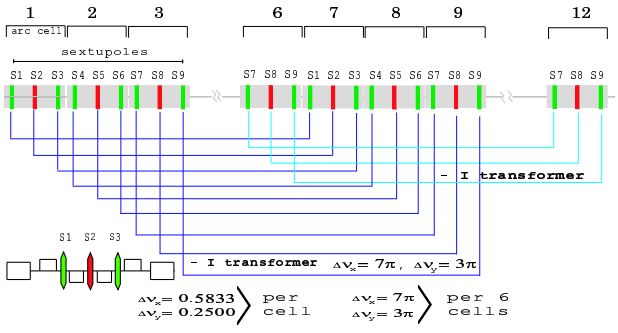

Figure 7: Second-order achromat of the damping ring

sextupole pairs are used for the chromatic correction. The uncorrected geometric aberrations introduced by the interlaced $-I$ sextupolar transformers are of third and higher order. The damping ring comprises two arcs, each of which consists of 48 cells. We have chosen 9 sextupole families located in 3 adjacent arc cells, as it is shown in Fig. 7 (three families for the vertical motion and six families for the horizontal motion). The horizontal and vertical phase advances over 6 cells with repetitive symmetry are 7π and 3π, respectively.

Taking into account phase advance per cell and the number of cells, one can see that we have assembled a complete second-order achromat using the interlaced $-I$ transformers. The second order achromat scheme provides an exact cancellation of all second-order geometric aberrations, since the X and Y phase advances per arc are multiples of 2π. For our lattice the phase advances over an arc are $\Delta\nu_x = 28 \times 2\pi$ and $\Delta\nu_y = 12 \times 2\pi$. It is obvious that all second-order geometric terms vanish, since the following

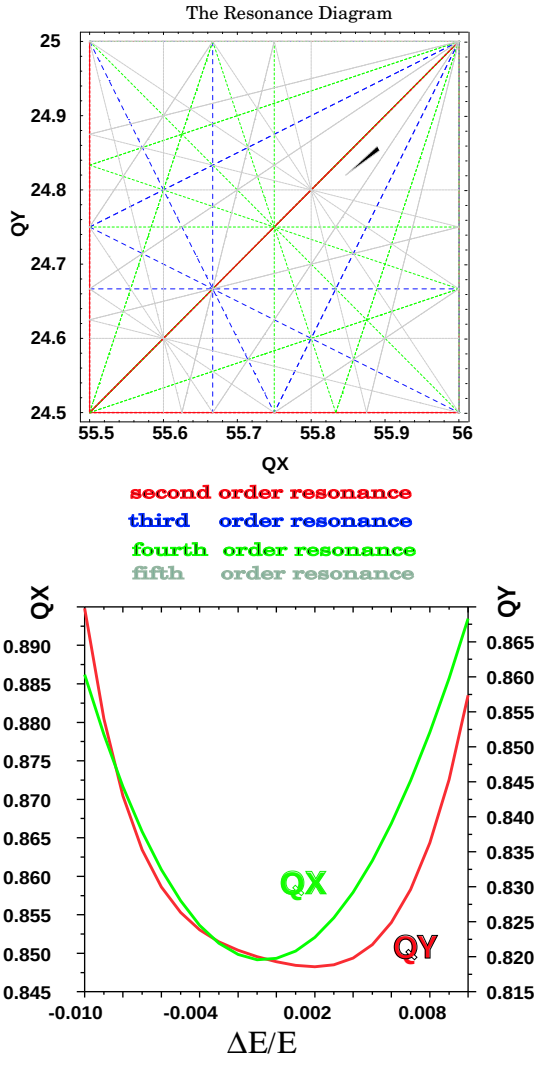

Figure 8: The tune shift versus momentum deviation (bottom) and the same on a resonance diagram (top).

two integrals are zero:

$$\int_0^L F_p \, e^{\pm i\psi} ds = 0 \qquad and \qquad \int_0^L F_p \, e^{\pm 3i\psi} ds = 0 \, .$$

Here the F_p functions are equal to the strength of an element multiplied by some power of the beta functions. Over the length of 12 cells and considering the sextupole elements, both integrals vanish. In the complex $i\psi$ and $3i\psi$ plane, the vector sums of the first and seventh cell etc. (2nd and 8th, 3rd and 9th, 6th with 12th) are zero. The first and second order chromatic aberrations are corrected by matching the strengths of 9 sextupole families. Without chromatic correction the natural first order chromaticities are -115 and -124 for the horizontal and vertical plane, respectively.

The strengths of the chromatic sextupoles are considerable (but their pole-tip fields do not exceed a value of 2 T, which we considered a reasonable upper bound), since the emittance requirements result in small beta and dispersion functions over the TME arc cell. The tune shift over a large momentum range of $\pm 1\%$ is shown in Fig. 8. The working point for zero momentum offset was chosen as $\nu_x/\nu_y \rightarrow 0.85/0.82$. A standard method to maximize the

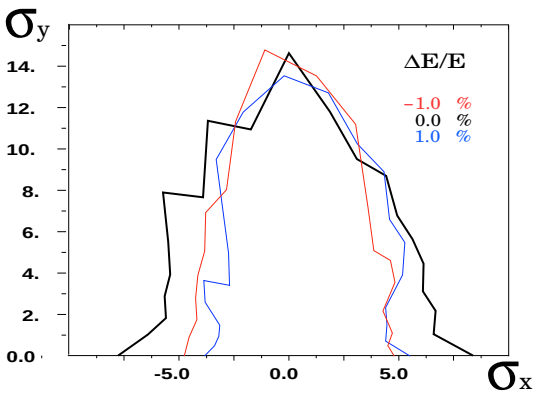

Figure 9: The dynamic aperture of the injected beam, as determined by particle tracking over 1000 turns.

dynamic aperture is to install harmonic sextupoles in non-dispersive sections. These allow reducing the tune shift with amplitude and compensating resonance-driving terms. In our present lattice, two families of harmonic sextupoles are used. Each consists of eight sextupoles, which are located in the wiggler sections. The harmonic sextupoles increase the dynamic aperture about two times, so that its value now corresponds to about six rms beam sizes for an on-momentum particle, as it is shown in Fig. 9. The dynamic aperture might be further improved by increasing the number of harmonic-sextupole families.

6 OUTLOOK

We have described the present design status of the CLIC damping ring. The ring comprises TME-cell arcs and two long FODO wiggler sections. The ring lattice has been optimized with respect to synchrotron radiation and intrabeam scattering, for a constant circumference.

The final equilibrium emittances have been estimated via numerical integration. The equilibrium transverse emittances fall a factor 2–3 short of the design target value, but are already below the emittances required at the CLIC collision point. The longitudinal emittance is slightly smaller than necessary. Recently the dynamic aperture has been optimized by using 9 families of chromatic correction, consisting of interleaved $-I$ pairs, and 2 additional harmonic families. It now exceeds 5–6 rms beam sizes at injection. The momentum acceptance of the lattice surpasses $\pm 1\%$.

We next plan to investigate the following three items: (1) the effect of alignment errors and beam-based tuning on the dynamic aperture, (2) the optimum choice of the emittance ratio, representing linear betatron coupling between the horizontal and vertical plane, which is an external input to the emittance computation, and (3) the potential for a transverse emittance reduction by increasing the length of the wiggler.

7 REFERENCES

[1] R. Assmann et al., G. Guignard (ed.), "A 3-TeV e^+e^- Linear Collider Based on CLIC Technology," CERN-2000-008 (2000).

[2] K. Hirata, "Effects of the Opening Angles to the Emittances," SLAC-AAS-NOTE-80 (1993).

[3] J.D. Bjorken, S.K. Mtingwa, "Intrabeam Scattering," Part. Accel. 13, 115–143 (1983).

[4] A. Piwinski, "Intrabeam Scattering," Proc. 9th Int. Conf. High Energy Acc., Stanford 1974, 405–409 (1974)

[5] L. Teng, "Minimizing the Emittance in Designing the Lattice of an Electron Storage Ring," FERMILAB-TM-1269 (1984).

[6] L. Teng, S.Y. Lee, "Theoretical Minimum Emittance Lattice for an Electron Storage Ring," (1991).

[7] J.P. Potier, L. Rivkin, "A Low Emittance Lattice for the CLIC Damping Ring," CERN-PS-97-020 (1997).

[8] J.P. Potier, T. Risselada, "Fundamental Design Principles of Linear Collider Damping Rings, with Application to CLIC,", EPAC 2000, Vienna, CERN-PS-2000-037-LP, CLIC-NOTE-439 (2000).

[9] P. Emma, T. Raubenheimer, "Systematic Approach to Damping Ring Design," Phys. Rev. ST Accel. Beams 4, 021001 (2001).

[10] A. Ropert, "High Brilliance lattice and the effects of ID," CERN Accelerator School, 6-13 April (1989).

[11] H. Wiedemann, "Low Emittance Storage Ring Design,"Lecture Notes in Physics 296, Texas (1986).

[12] J.M. Jowett, T. Risselada, F. Zimmermann, H. Owen "Damping Rings for CLIC," PAC2001, Chicago (2001).

[13] M. Korostelev, F. Zimmermann, "Optimization of CLIC Damping Ring Design Parameters," EPAC 2002 Paris (2002).